

---

# Flash3D: Feed-Forward Generalisable 3D Scene Reconstruction from a Single Image

---

**Stanislaw Szymanowicz\***  
VGG, University of Oxford  
stan@robots.ox.ac.uk

**Eldar Insafutdinov\***  
VGG, University of Oxford  
eldar@robots.ox.ac.uk

**Chuanxia Zheng\***  
VGG, University of Oxford  
cxzheng@robots.ox.ac.uk

**Dylan Campbell**  
Australian National University  
dylan.campbell@anu.edu.au

**João F. Henriques**  
VGG, University of Oxford  
joao@robots.ox.ac.uk

**Christian Rupprecht**  
VGG, University of Oxford  
chrisr@robots.ox.ac.uk

**Andrea Vedaldi**  
VGG, University of Oxford  
vedaldi@robots.ox.ac.uk

## Abstract

In this paper, we propose Flash3D, a method for scene reconstruction and novel view synthesis from a single image which is both very generalisable and efficient. For generalisability, we start from a ‘foundation’ model for monocular depth estimation and extend it to a full 3D shape and appearance reconstructor. For efficiency, we base this extension on feed-forward Gaussian Splatting. Specifically, we predict a first layer of 3D Gaussians at the predicted depth, and then add additional layers of Gaussians that are offset in space, allowing the model to complete the reconstruction behind occlusions and truncations. Flash3D is very efficient, trainable on a single GPU in a day, and thus accessible to most researchers. It achieves state-of-the-art results when trained and tested on RealEstate10k. When transferred to *unseen* datasets like NYU it outperforms competitors by a large margin. More impressively, when transferred to KITTI, Flash3D achieves better PSNR than methods trained specifically on that dataset. In some instances, it even outperforms recent methods that use multiple views as input. Code, models, demo, and more results are available at <https://www.robots.ox.ac.uk/~vgg/research/flash3d/>.

## 1 Introduction

We consider the problem of reconstructing photorealistic 3D scenes from a single image in just one forward pass of a network. This is a challenging task because scenes are complex and monocular reconstruction is ill-posed. Unambiguous geometric cues, such as triangulation, are unavailable in the monocular setting, and there is no direct evidence of the occluded parts of the scene.

This problem is closely related to monocular depth estimation [4, 6, 7, 16, 20, 33, 34, 46, 47, 56, 59, 90], which is a mature area. It is now possible to accurately estimate metric depth with excellent cross-domain generalisation [47, 90, 91]. However, while depth estimators predict the 3D shape of the nearest visible surfaces, they do not provide any *appearance* information, nor an estimate of the occluded or out-of-frame parts of the scene. Depth alone is insufficient to accurately solve tasks such as *novel view synthesis* (NVS), which additionally require modelling unseen regions and view-dependent appearance.

While methods for monocular scene reconstruction exist [36, 74, 85], they mostly operate in a ‘closed-world’ setting where they are trained anew for each considered dataset. In contrast, modern

---

\*denotes equal contribution

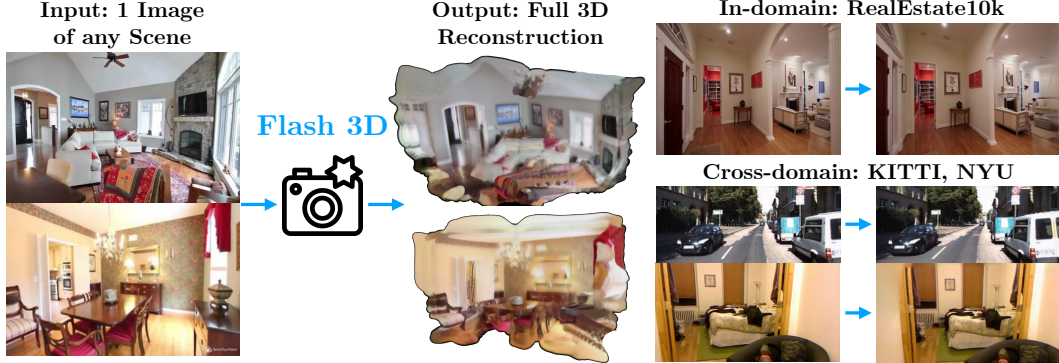


Figure 1: **Flash3D** reconstructs the 3D (*not* 2.5D) scene structure and appearance from just a single image ‘in a flash’, enabling accurate novel view synthesis. Trained on just one dataset, it generalises to new, different datasets and unknown scenes.

depth predictors generalise well to new datasets at inference time. Furthermore, current monocular scene reconstructors are often slow or incur a high computational memory cost due to volumetric rendering [36] and implicit representations [92].

Very recently, Szymanowicz et al. [68] introduced the Splatter Image (SI), a method for fast monocular reconstruction of individual objects that builds upon the success of Gaussian Splatting [31]. The approach is simple: predict the parameters of a coloured 3D Gaussian for each input image pixel using a standard image-to-image neural network architecture. The resulting Gaussian mixture was shown to reconstruct objects well, including unobserved surfaces. In part, this was due to the fact that SI is able to use some of the “background pixels” to model the occluded parts of the object. However, in scene reconstruction, there is not such a reservoir of background pixels, which poses a challenge for the method. In contrast, pixelSplat [9], MVSplat [11], latentSplat [83] and GS-LRM [95], which share a similar design, were designed for scene reconstruction; however, they address the binocular reconstruction problem, requiring *two* images of the scene captured from different *known* viewpoints. We instead consider the more challenging monocular setting, since it is more generally applicable and does not require camera extrinsics, which is a challenging research problem on its own [78, 80, 94].

In this work, we introduce a new, simple, efficient and performant approach for monocular scene reconstruction called *Flash3D*. This is based on two key ideas. First, we address the issue of *generalisation* which limits current feed-forward monocular scene reconstructors. The aim is for Flash3D to work on any scene, not just on scenes similar to the ones in the training set. Analogous open-ended models are often called foundation models and require massive training datasets and computational resources unavailable to most research groups. A similar problem exists in 3D object reconstruction and generation [35, 37, 40, 41, 60, 97], where it is addressed by extending to 3D an existing foundation 2D image or video generator [5, 13, 19, 48, 53]. Here, we posit that scene reconstruction can also benefit from building on an existing foundation model, but opt for a monocular depth predictor as a more natural choice. We show, in particular, that by building on a high-quality depth predictor [47], we can achieve excellent generalisation to new datasets, to the point that our 3D reconstructions are more accurate than those of models trained specifically on those test domains.

Second, we improve feed-forward per-pixel Gaussian splatting for monocular scene reconstruction. As noted, applied to single objects, a per-pixel reconstructor can use the reservoir of background pixels to model the hidden parts of the object, which is not possible when reconstructing a full scene. Our solution is to predict multiple Gaussians per pixel, where only the first Gaussian along each ray is encouraged to conform to the depth estimate and thus model the visible part of the scene. This is analogous to a layered representation [1, 3, 36, 58, 74, 76] and multi-Gaussian sampling in pixelSplat [9]. However, in our case Gaussians are deterministic, not limited to specific depth ranges, and the model is free to shift Gaussians off the ray to model occluded or truncated parts of the scene.

Overall, Flash3D is a simple and highly-performant monocular scene reconstruction pipeline. Empirically, we find that Flash3D can (a) render high-quality images of the reconstructed 3D scene, (b) operate on a wide range of scenes, both indoor and outdoor; and (c) reconstruct occluded regions, which would not be possible with depth estimation alone or with naïve extensions of it. Flash3D achieves state-of-the-art novel view synthesis accuracy on all metrics on the RealEstate10K [72].

More impressively the same, frozen model also achieves state-of-the-art accuracy when transferred to NYU [61] and KITTI [18] (in PSNR). Furthermore, in an extrapolation setting, our reconstructions can even be more accurate than those of binocular methods like pixelSplat [9] and latentSplat [83] that use two images of the scene instead of one, and are thus at a significant advantage.

In addition to the quality of the reconstructions, shown in Fig. 1, Flash3D is very efficient to evaluate and, most importantly, to train. For instance, we use 1/64<sup>th</sup> of the GPU resources of prior works like MINE [36]. By achieving state-of-the-art results while using modest computational resources for training, this opens the research area up to a wider range of researchers.

## 2 Related Work

**Monocular feed-forward reconstruction.** Like our approach, monocular feed-forward reconstructors work by passing a single image of the scene through a neural network to output a 3D reconstruction directly. For *scenes*, the works of [74–76] and MINE [36] do so by predicting multi-plane images [72], and [85] uses neural radiance fields [43, 62]. Our method outperforms them in terms of speed and generalisation. Like our work, SynSin [84] uses a monocular depth predictor to reconstruct a scene; however, its reconstructions are incomplete and require a rendering network to improve the final novel views. In contrast, our approach outputs a high-quality 3D reconstruction which can be directly rendered with Gaussian Splatting [31]. For *objects*, a notable example is Large Reconstruction Model (LRM) [27], which obtains high-quality monocular reconstruction with a very large, and very expensive to train, model. The most related work to ours is Splatter Image [68] that uses Gaussian Splatting [31] for efficiency. Our approach also uses Gaussian Splatting as a representation, but does so for scenes rather than objects, which presents different challenges.

**Few-view feed-forward reconstruction.** A less challenging but still important case is few-view feed-forward reconstruction, where reconstruction requires two or more images taken from known viewpoints. Early examples used neural radiance fields (NeRF) [43] as 3D representation of *objects* [12, 25, 29, 38, 51, 79, 92] and scenes [12, 14, 88]. These methods implicitly learn to match points between views; the works of [10, 93] makes point matching more explicit. While many few-view reconstructors estimate the 3D shape of the object as an opacity field, an alternative is to directly predict new views [44, 55, 65, 66] of *scenes* with no explicit volumetric reconstruction, a concept pioneered by Light Field Networks [63]. Other works use instead multi-plane images from narrow baseline stereo pairs [64, 72] and few views [30, 42]. More related to our approach, pixel-Splat [9], latentSplat [83] and MVSSplat [11] reconstruct scenes from a pair of images. They utilise cross-view attention to efficiently share information and predict Gaussian mixtures to represent the scene geometry. Other very recent feed-forward approaches [69, 89, 95] combine LRM and Gaussian Splatting for reconstruction from a small number of images. We address *monocular* reconstruction instead, which is a much harder problem due to lack of geometric cues from triangulation.

**Iterative reconstruction.** Iterative or optimisation-based methods reconstruct from one or more images by iteratively fitting a 3D model to them. Due to their iterative nature, and the need to render the 3D model to fit it to the data, they are generally much slower than feed-forward approaches. DietNeRF [28] regularises reconstruction using language models, RegNeRF [45] and RefNeRF [77] use handcrafted regularisers, and SinNeRF [87] uses monocular depth. RealFusion [40] uses an image diffusion model as a prior for monocular reconstruction based on slow score distillation sampling iterations [49]. Numerous follow-ups took a similar path [70, 86]. Convergence speed and robustness can be improved by using multi-view aware generators [23, 37, 41, 73, 82, 97]. Approaches like Viewset Diffusion [67] and RenderDiffusion [2] fuse 3D reconstruction with diffusion-based generation, which can reduce but not eliminate the cost of iterative generation. In contrast, our approach is feed-forward and therefore significantly faster, close to real-time (10fps). Some approaches generate novel views in a feed-forward manner, but iteratively and autoregressively, one view at a time. Examples include PixelSynth [52], extending SynSin, GeNVS [8], and Text2Room [26]. In contrast, we generate the final 3D reconstruction in a single feed-forward pass.

**Monocular depth prediction.** Our method is based on monocular depth estimation [4, 6, 7, 15, 16, 20, 21, 33, 34, 46, 50, 56, 59, 90, 98], where metric or relative depth is predicted for every image pixel for a given image. By learning visual depth cues from large datasets, often with self-supervision, these approaches have demonstrated high accuracy and the capacity to generalise across datasets. While our method is agnostic to the depth predictor used, we use one of the state-of-the-art metric depth estimators, UniDepth [47], for our experiments.

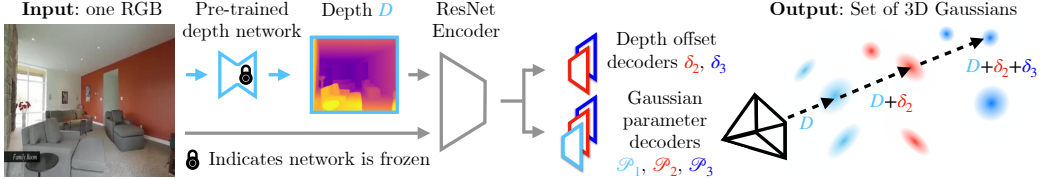


Figure 2: **Overview of Flash3D.** Given a single image  $I$  as input, Flash3D first estimates the metric depth  $D$  using a frozen off-the-shelf network [47]. Then, a ResNet50-like encoder–decoder network predicts a set of shape and appearance parameters  $\mathcal{P}$  of  $K$  layers of Gaussians for every pixel  $u$ , allowing unobserved and occluded surfaces to be modelled. From these predicted components, the depth can be obtained by summing the predicted (positive) offsets  $\delta_i$  with the predicted monocular depth  $D$ , allowing the mean vector for every layer of Gaussians to be computed. This strategy ensures that the layers are depth-ordered, encouraging the network to model occluded surfaces.

### 3 Method

Let  $I \in \mathbb{R}^{3 \times H \times W}$  be an RGB image of a scene. Our goal is to learn a neural network  $\Phi$  that takes as input  $I$  and predicts a representation  $\mathcal{G} = \Phi(I)$  of the 3D content of the scene, both in terms of 3D geometry and photometry. We first discuss the background and baseline model in Section 3.1, then introduce our layered multi-Gaussian predictor in Section 3.2, and finally discuss the use of monocular depth prediction as a prior in Section 3.2.

#### 3.1 Background: Scene reconstruction from a single image

**Representation: scenes as sets of 3D Gaussians.** The scene representation  $\mathcal{G} = \{(\sigma_i, \mu_i, \Sigma_i, c_i)\}_{i=1}^G$  is a set of 3D Gaussians [31], where  $\sigma_i \in [0, 1]$  is the opacity,  $\mu_i \in \mathbb{R}^3$  is the mean,  $\Sigma_i \in \mathbb{R}^{3 \times 3}$  is the covariance matrix, and  $c_i : \mathbb{S}^2 \rightarrow \mathbb{R}^3$  is the radiance function (directional colour) of each component. Let  $g_i(\mathbf{x}) = \exp\left(-\frac{1}{2}(\mathbf{x} - \boldsymbol{\mu}_i)^\top \Sigma_i^{-1}(\mathbf{x} - \boldsymbol{\mu}_i)\right)$  be the corresponding (un-normalised) Gaussian function. The colours of the Gaussians are generally represented using spherical harmonics, so that  $[c_i(\boldsymbol{\nu})]_j = \sum_{l=0}^L \sum_{m=-l}^l c_{ijlm} Y_{lm}(\boldsymbol{\nu})$ , where  $\boldsymbol{\nu} \in \mathbb{S}^2$  is a view direction and  $Y_{lm}$  are the spherical harmonics of various orders  $m$  and degrees  $l$ . The Gaussian mixture  $\mathcal{G}$  defines the opacity and colour functions of a radiance field:  $\sigma(\mathbf{x}) = \sum_{i=1}^G \sigma_i g_i(\mathbf{x})$ ,  $c(\mathbf{x}, \boldsymbol{\nu}) = \sum_{i=1}^G c_i(\boldsymbol{\nu}) \sigma_i g_i(\mathbf{x}) / \sum_{i=1}^G \sigma_i g_i(\mathbf{x})$ , where  $\sigma(\mathbf{x})$  is the opacity at 3D location  $\mathbf{x} \in \mathbb{R}^3$  and  $c(\mathbf{x}, \boldsymbol{\nu})$  is the radiance at  $\mathbf{x}$  in direction  $\boldsymbol{\nu} \in \mathbb{S}^2$  towards the camera.

The field is rendered into an image  $J$  by integrating the radiance along the line of sight using the *emission-absorption* [39] equation  $J(\mathbf{u}) = \int_0^\infty c(\mathbf{x}_t, \boldsymbol{\nu}) \sigma(\mathbf{x}_t) \exp\left(-\int_0^t \sigma(\mathbf{x}_\tau) d\tau\right) dt$ , where  $\mathbf{x}_t = \mathbf{x}_0 - t\boldsymbol{\nu}$  is the ray originating at the camera centre  $\mathbf{x}_0$  and propagating towards the pixel  $\mathbf{u}$  in the direction  $-\boldsymbol{\nu}$ . The key contribution of Gaussian Splatting [31] is to approximate this integral very efficiently, implementing a differentiable rendering function  $\hat{J} = \text{Rend}(\mathcal{G}, \pi)$  which takes as input the Gaussian mixture  $\mathcal{G}$  and viewpoint  $\pi$  and returns an estimate  $\hat{J}$  of the corresponding image.

**Monocular reconstruction.** Following [68], the output  $\Phi(I) \in \mathbb{R}^{C \times H \times W}$  of the neural network is a tensor that specifies, for each pixel  $\mathbf{u} = (u_x, u_y, 1)$ , the parameters of a coloured Gaussian, consisting of the opacity  $\sigma$ , the depth  $d \in \mathbb{R}_+$ , the offsets  $\Delta \in \mathbb{R}^3$ , the covariance  $\Sigma \in \mathbb{R}^{3 \times 3}$  expressed as rotation and scale (seven parameters, using quaternions for rotation), and the parameters of the colour model  $c \in \mathbb{R}^{3(L+1)^2}$  where  $L$  is the order of the spherical harmonics. The mean of the Gaussian is then given by  $\boldsymbol{\mu} = K^{-1}\mathbf{u}d + \Delta$ , where  $K = \text{diag}(f, f, 1) \in \mathbb{R}^{3 \times 3}$  is the camera calibration matrix and  $f$  its focal length. Hence, there are  $C = 1 + 1 + 3 + 7 + 3(L+1)^2 = 12 + 3(L+1)^2$  parameters predicted for each pixel. The model  $\Phi$  is trained using triplets  $(I, J, \pi)$  where  $I$  is an input image,  $J$  is a target image, and  $\pi$  is the relative camera pose. To learn the network parameters, one simply minimises the rendering loss  $\mathcal{L}(\mathcal{G}, \pi, J) = \|\text{Rend}(\mathcal{G}, \pi) - J\|$ .

#### 3.2 Monocular feed-forward multi-Gaussians

For generalisation, we propose to build Flash3D on a high-quality pre-trained model trained on a large amount of data. Specifically, given the similarities between monocular scene reconstruction and monocular depth estimation, we use an off-the-shelf monocular depth predictor  $\Psi$ . This model takes

as input an image  $I$  and returns a depth map  $D = \Psi(I)$ , where  $D \in \mathbb{R}_+^{H \times W}$  is a matrix of depth values, as explained next.

**Baseline architecture.** Given an image  $I$  and estimated depth map  $D$ , our baseline model consists of an additional network  $\Phi(I, D)$  that takes as input the image and the depth map and returns the required per-pixel Gaussian parameters. In more detail, for each pixel  $\mathbf{u}$ , the entry  $[\Phi(I, D)]_{\mathbf{u}} = (\sigma, \Delta, s, \theta, c)$  consists of the opacity  $\sigma \in \mathbb{R}_+$ , the displacement  $\Delta \in \mathbb{R}^3$ , the scale  $s \in \mathbb{R}^3$ , the quaternion  $\theta \in \mathbb{R}^4$  parametrising the rotation  $R(\theta)$ , and the colour parameters  $c$ . The covariance of each Gaussian is given by  $\Sigma = R(\theta)^\top \text{diag}(s)R(\theta)$  and the mean is given [68] by  $\mu = (u_x d/f, u_y d/f, d) + \Delta$ , where  $f$  is the focal length of the camera (either known or also estimated by  $\Psi$ ) and the depth  $d = D(\mathbf{u})$  is from the depth map. The network  $\Phi$  is a U-Net [54] utilising ResNet blocks [24] for encoding and decoding, denoted  $\Phi_{\text{enc}}$  and  $\Phi_{\text{dec}}$  respectively. The decoder network thus outputs a tensor  $\Phi_{\text{dec}}(\Phi_{\text{enc}}(I, D)) \in \mathbb{R}^{(C-1) \times H \times W}$ . Note that the network output has  $C - 1$  channels only, as depth is taken directly from  $\Psi$ . Please see the supplement for full details.

**Multi-Gaussian prediction.** While the Gaussians in the model above have the ability to be offset from the corresponding pixel’s ray, each Gaussian tends naturally to model the portion of the object that projects onto that pixel. Szymanowicz et al. [68] note that, for individual objects, there is a large number of background pixels that are not associated with any object surface, and these can be repurposed by the model to capture the unobserved parts of the 3D object. However, this is not the case for scenes, where the goal is to reconstruct every input pixel, and beyond.

Since there are no “idle” pixels, it is difficult for the model to repurpose some of the Gaussians to model the 3D scene around occlusions and beyond the image field-of-view. Hence, we propose to predict a small number  $K > 1$  of different Gaussians for each pixel.

Conceptually, given an image  $I$  and an estimated depth map  $D$ , our network predicts a set of shape, location and appearance parameters  $\mathcal{P} = \{(\sigma_i, \delta_i, \Delta_i, \Sigma_i, c_i)\}_{i=1}^K$  for every pixel  $\mathbf{u}$ , where the depth of the  $i^{\text{th}}$  Gaussian is given by

$$d_i = d + \sum_{j=1}^i \delta_j, \quad (1)$$

where  $d = D(\mathbf{u})$  is the predicted depth at pixel  $\mathbf{u}$  in depth map  $D$  and  $\delta_1 = 0$  is a constant. Note that, since the depth offset  $\delta_i$  cannot be negative, this ensures that subsequent Gaussian layers are “behind” previous ones and encourages the network to model occluded surfaces. The mean of the  $i^{\text{th}}$  Gaussian is then given by  $\mu_i = (u_x d_i/f, u_y d_i/f, d_i) + \Delta_i$ . In practice, we find  $K = 2$  to be a sufficiently expressive representation.

**Reconstructing beyond the border with padding.** As we show empirically, it is important for the network to be able to model 3D content just outside its field-of-view. While the multiple Gaussian layers help in this regard, there is a particular need for additional Gaussians near the image border (*e.g.*, for good new view synthesis when the camera retracts). To facilitate obtaining such Gaussians, the encoder  $\Phi_{\text{enc}}$  starts by *padding* the input image and depth  $(I, D)$  with  $P > 0$  pixels on each side, so that the outputs  $\Phi_k(I, D) \in \mathbb{R}^{(C-1) \times (H+2P) \times (W+2P)}$  are larger than the inputs.

## 4 Experiments

We design our experiments to support four key findings, with each section dedicated to one finding. We begin with the most important result: cross-dataset generalisation—leveraging a monocular depth prediction network and training on a single dataset results in good reconstruction quality on other datasets (Section 4.2). Second, we establish that Flash3D serves as an effective representation for single-view 3D reconstruction by comparing against methods specifically designed for this task (Section 4.3). Third, we go as far as to show that the prior learned by single-view Flash3D is as strong as that learned by two-view methods (Section 4.4). Finally, we show via ablation studies how each design choice contributes to performance Flash3D (Section 4.5) and analyse outputs from Flash3D to gain insight into its inner workings.

### 4.1 Experiment settings

**Datasets.** Flash3D is trained only on the large-scale RealEstate10k [72] dataset, containing real estate videos from YouTube. We follow the default training/testing split with 67,477 scenes for

Table 1: **Cross-Domain Novel View Synthesis.** We evaluate NVS accuracy on datasets not used in training of our method. We outperform baselines which were trained on KITTI specifically. Here, cross-domain (CD) denotes that the method was not trained on the dataset being evaluated.

| Method                    | CD           | KITTI           |                 |                    | NYU          |                 |                 |                    |
|---------------------------|--------------|-----------------|-----------------|--------------------|--------------|-----------------|-----------------|--------------------|
|                           |              | PSNR $\uparrow$ | SSIM $\uparrow$ | LPIPS $\downarrow$ | CD           | PSNR $\uparrow$ | SSIM $\uparrow$ | LPIPS $\downarrow$ |
| LDI [76]                  | $\times$     | 16.50           | 0.572           | -                  | -            | -               | -               | -                  |
| SV-MPI [74]               | $\times$     | 19.50           | 0.733           | -                  | -            | -               | -               | -                  |
| BTS [85]                  | $\times$     | 20.10           | 0.761           | 0.144              | -            | -               | -               | -                  |
| MINE [36]                 | $\times$     | 21.90           | <b>0.828</b>    | <b>0.112</b>       | $\checkmark$ | 24.33           | 0.745           | 0.202              |
| UniDepth w/ $\mathcal{U}$ | $\checkmark$ | 20.86           | 0.774           | 0.154              | $\checkmark$ | 22.54           | 0.732           | 0.212              |
| Flash3D (Ours)            | $\checkmark$ | <b>21.96</b>    | 0.826           | 0.132              | $\checkmark$ | <b>25.45</b>    | <b>0.774</b>    | <b>0.196</b>       |

training and 7,289 for testing. Once Flash3D is trained, we assess its effectiveness across various datasets, discussed in detail in each section. For details of the evaluation protocols, see the appendix.

**Metrics.** For quantitative results, we report the standard image quality metrics, including pixel-level PSNR, patch-level SSIM, and feature-level LPIPS.

**Compared methods.** We compare with several state-of-the-art approaches that are designed specifically for single-view scene reconstruction, including LDI [76], Single-View MPI [74], SynSin [84], BTS [85] and MINE [36]. We include a comparison to our adaptation of Splatter Image [68] to show that our method is much better suited to general scenes, as well as a comparison to ray-wise unprojection  $\mathcal{U}$  of the input colours to the locations predicted by the depth network. Finally, while not a fair comparison, we also compare with state-of-the-art two-view novel view synthesis methods, including [14], pixelSplat [9], MVSplat [11], and latentSplat [83].

**Implementation details.** Flash3D comprises a pre-trained UniDepth [47] model, a ResNet50 [24] encoder, alongside multiple depth offset decoders and Gaussian decoders. The entire model is trained on a single A6000 GPU for 40,000 iterations with batch size 16. The training is remarkably efficient, completed in one day on a single A6000 GPU. Given that UniDepth remains frozen during training, we can expedite the training by pre-extracting depth maps for the entire dataset. With this, Flash3D can be trained to achieve state-of-the-art quality on a *single A6000 GPU in 16 hours*.

## 4.2 Cross-domain novel view synthesis

**Datasets.** To evaluate the cross-domain generalisation ability, we directly evaluate performance on unseen outdoor (KITTI [17]) and indoor (NYU [61]) datasets. For KITTI, we follow standard benchmarks with a well-established protocol for evaluation, with 1,079 images for testing. For NYU, we formed a new protocol, with 250 source images for testing (see supp. mat for details). We evaluate all methods in the same manner. We verified that Unidepth [47] was not trained on these datasets.

To the best of our knowledge, we are the first to report performance on feed-forward cross-domain monocular reconstruction. We consider two challenging comparisons. First, we evaluate Flash3D and the current state-of-the-art [36] on NYU, an indoor dataset that is similar in nature to RE10k, yet unseen in training. In Table 1, we observe that our method performs significantly better on this transfer experiment, despite the domain gap being relatively small. This suggests that prior works do not generalise as well as our method. Second, we compare our method on KITTI in Table 1, where it performs on par with the state-of-the-art that was trained on this dataset. Indeed, Flash3D outperforms the others with respect to PSNR, despite being trained only on an indoor dataset. This suggests that leveraging a pretrained depth network has allowed our network to learn an extremely strong shape and appearance prior that is even more accurate than learning on this dataset directly.

## 4.3 In-domain novel view synthesis

We perform an in-domain evaluation on RealEstate10k [72], following the same protocol as prior works [36]. We evaluate the quality of zero-shot reconstruction and compare performance on an in-domain dataset, RealEstate10k. We evaluate the quality of reconstruction through novel view synthesis metrics as that is the only ground-truth data available in this dataset. RealEstate10k evaluates the quality of reconstructions at different distances between the source and the target, as a smaller distance makes the task easier. In Table 2, we observe that we achieve state-of-the-art results on this mature benchmark across all distances between the source and the target. Further

Table 2: **In-domain Novel View Synthesis.** Our model shows state-of-the-art in-domain performance on RealEstate10k on small, medium and large baseline ranges.

| Model               | PSNR $\uparrow$ | 5 frames        |                    |                 | 10 frames       |                    |                 | $\mathcal{U}[-30, 30]$ frames |                    |  |
|---------------------|-----------------|-----------------|--------------------|-----------------|-----------------|--------------------|-----------------|-------------------------------|--------------------|--|
|                     |                 | SSIM $\uparrow$ | LPIPS $\downarrow$ | PSNR $\uparrow$ | SSIM $\uparrow$ | LPIPS $\downarrow$ | PSNR $\uparrow$ | SSIM $\uparrow$               | LPIPS $\downarrow$ |  |
| Syn-Sin [84]        | -               | -               | -                  | -               | -               | -                  | 22.30           | 0.740                         | -                  |  |
| SV-MPI [74]         | 27.10           | 0.870           | -                  | 24.40           | 0.812           | -                  | 23.52           | 0.785                         | -                  |  |
| BTS [85]            | -               | -               | -                  | -               | -               | -                  | 24.00           | 0.755                         | 0.194              |  |
| Splatter Image [68] | 28.15           | 0.894           | 0.110              | 25.34           | 0.842           | 0.144              | 24.15           | 0.810                         | 0.177              |  |
| MINE [36]           | 28.45           | 0.897           | 0.111              | 25.89           | 0.850           | 0.150              | 24.75           | 0.820                         | 0.179              |  |
| Flash3D (Ours)      | <b>28.46</b>    | <b>0.899</b>    | <b>0.100</b>       | <b>25.94</b>    | <b>0.857</b>    | <b>0.133</b>       | <b>24.93</b>    | <b>0.833</b>                  | <b>0.160</b>       |  |

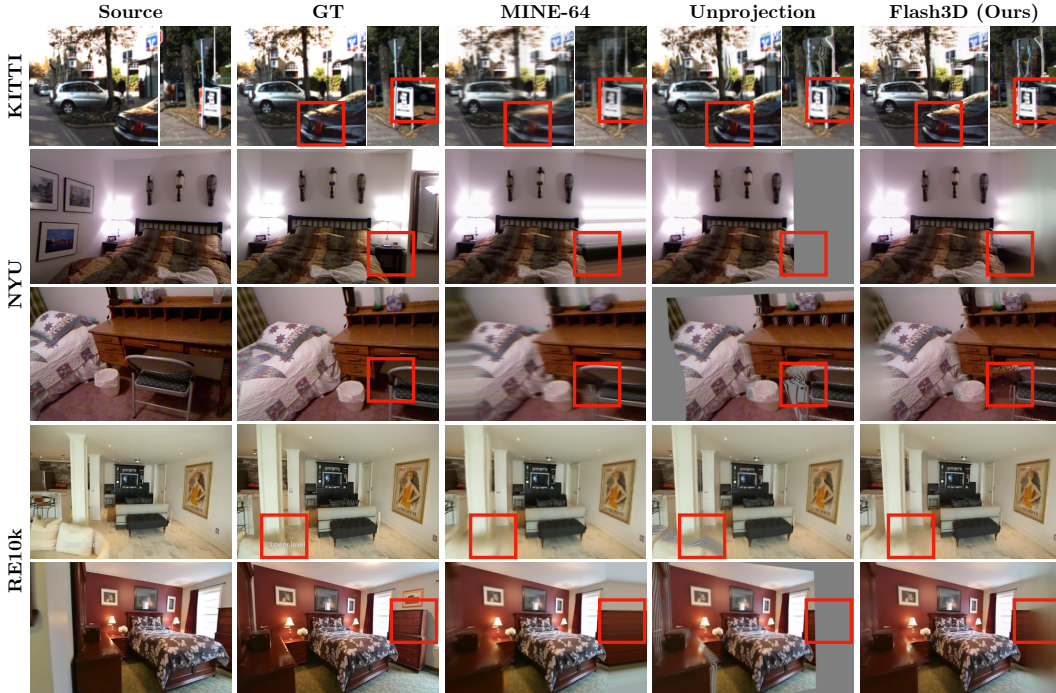


Figure 3: **Qualitative comparison of monocular reconstruction** on all datasets. Flash3D (Ours, right column) is sharper (top row, car’s back) than state-of-the-art MINE [36] despite Flash3D not training on KITTI. This is thanks to leveraging a depth predictor which, when used on its own (fourth column), cannot represent occluded regions (third row, fourth row). As well as representing occluded regions better than MINE (first row, third row and fourth row), Flash3D also fills in better explanations of regions outside the source camera frustum (second row, fifth row).

analysis in Fig. 3 reveals that our method’s reconstructions are sharper and more accurate than prior state-of-the-art [36], despite being trained on an order of magnitude fewer GPUs (1 vs. 64).

#### 4.4 Comparison to few-view novel view synthesis

**Datasets.** To further evaluate the effectiveness of Flash3D, we conducted assessments using the pixelSplat [9] split for interpolation and the latentSplat [83] split for extrapolation.

Unlike existing two-view methods that typically assess interpolation between two source views, Flash3D consistently performs extrapolation from a single view. The results are reported in Table 3. Here, Flash3D cannot outperform two-view approaches on the interpolation task, due to receiving less information. However, Flash3D surpasses all previous state-of-the-art two-view methods at view extrapolation. This highlights the utility of the multi-layer Gaussian representation of our approach at capturing and modelling unseen areas.

Table 3: **Comparison with Two-view Methods.** We compare on the split used by pixelSplat [9] for two-view interpolation and on the split used by latentSplat [83] for extrapolation. We take the view closest to the target as the source. Our method uses a *single* view and still extrapolates better.

| Method           | Input Views | RE10k Interpolation |                 |                    | RE10k Extrapolation |                 |                    |
|------------------|-------------|---------------------|-----------------|--------------------|---------------------|-----------------|--------------------|
|                  |             | PSNR $\uparrow$     | SSIM $\uparrow$ | LPIPS $\downarrow$ | PSNR $\uparrow$     | SSIM $\uparrow$ | LPIPS $\downarrow$ |
| Du et al [14]    | 2           | 24.78               | 0.820           | 0.213              | 21.83               | 0.790           | 0.242              |
| pixelSplat [9]   | 2           | 26.09               | 0.864           | 0.136              | 21.84               | 0.777           | 0.216              |
| latentSplat [83] | 2           | 23.93               | 0.812           | 0.164              | 22.62               | 0.777           | 0.196              |
| MVSplat [11]     | 2           | <b>26.39</b>        | <b>0.869</b>    | <b>0.128</b>       | 23.04               | 0.813           | <b>0.185</b>       |
| Flash3D (Ours)   | <b>1</b>    | 23.87               | 0.811           | 0.185              | <b>24.10</b>        | <b>0.815</b>    | <b>0.185</b>       |

#### 4.5 Ablation study and analysis

**Ablation study.** We ablate our method for in-domain and cross-domain settings in Table 4, focusing on the following questions. **Q1:** Is leveraging a monocular depth predictor useful in the task of reconstructing appearance and geometry of scenes? **Q2:** If yes, is it sufficient on its own, *i.e.*, is learning shape and appearance parameters necessary for scene reconstruction with 3D Gaussians?

*Importance of depth predictor.* We remove the pretrained depth network that predicts depth  $D$ , instead estimating it jointly with all other parameters. First, in Table 4 we observe that this leads to a significant drop in performance compared to Flash3D, indicating that the depth network contains important cues that had already been learned. Moreover, the third row of Table 4 indicates that without the depth network, 2 layers of Gaussians per pixel performs *worse* than using just one layer. We hypothesise that the depth network plays an important role in avoiding local optima that were reported to limit the learning capabilities of primitive-based methods [9]. Qualitatively, the fourth column in Fig. 4 illustrates that removing the depth network makes it challenging to learn accurate geometries of walls (orange wall is bent) and object boundaries (bed has an incorrect shape).

*Importance of extending beyond depth prediction.* Here we remove the learned parts of our network. First, we use only one layer of Gaussians, and predict parameters  $\mathcal{P}_1$  corresponding to the depth  $D$  predicted by the pre-trained depth network. This also results in a drop in performance in Table 4. We then go further and remove the network that predicts  $\mathcal{P}_1$ , removing learning altogether. Novel views are simply rendered from source view colours backprojected with the depths  $D$ . This understandably drops the performance even further. In Fig. 4 we observe that these drops are due to the 1-layer method not representing occluded parts of the scene. The last column in Fig. 4 illustrates that the holes are significant when using only depth unprojection, and can be partially mitigated when learning shapes  $\mathcal{P}_1$  due to the network being able to stretch the Gaussians at depth discontinuities.

**Analysis.** Fig. 5 analyses the mechanism through which the Gaussian layers form a full reconstruction of the scene. We visualise the depth of each of the layers,  $D$  and  $D + \delta_2$ , multiplied by the opacity  $\sigma_1, \sigma_2$  of the corresponding Gaussians, illustrating how much they are used when rendering the scene. In Fig. 5, the more saturated the colour, the more opaque the Gaussian (black is fully transparent). We observe that the first layer has the most opaque Gaussians at object boundaries (wall, cabinet) and at complicated geometries (chair), indicating that these are the regions where the depth prediction network is the most useful. This is further supported by Fig. 4 where removing the depth network impaired reconstruction in exactly the same regions. Leveraging the depth network at object boundaries results in crisp, accurate geometries at small baselines (fourth column). Interestingly, the network ignores the depth prediction for windows, which are consistently incorrect. Next, we analyse where the second layer of Gaussians places its predictions. In the third column of Fig. 5, where the network observes a wall, the second layer of Gaussians is placed at larger depth. These Gaussians are observed when the camera motion (baseline) is large, and are shown to have a reasonable appearance in Fig. 5 (right column). The last column in Fig. 5 additionally reveals a limitation of our method. It is a deterministic, regressive model of structure and appearance, and thus produces blurry renderings in presence of ambiguity: when baselines are very large, in occluded regions or when camera moves backward. Blurriness could be reduced with additional losses (perceptual [96] or adversarial [22]). Alternatively, our method could be incorporated as conditioning within a framework similar to [8] or as the reconstructor in a diffusion-based feedforward 3D generation framework [67, 71].

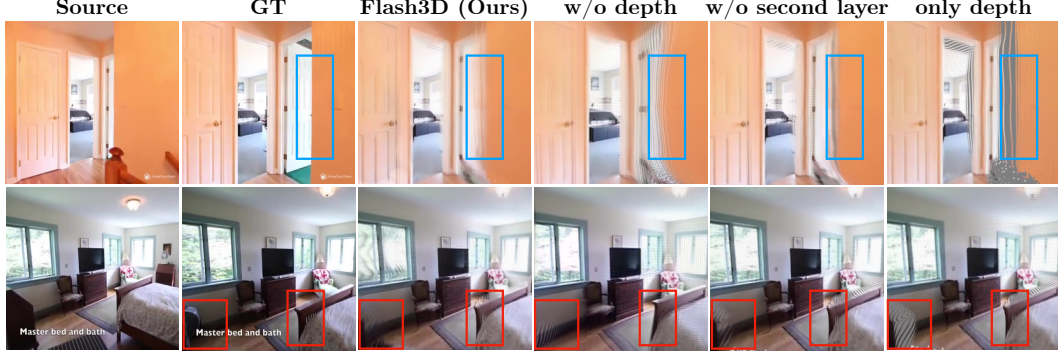


Figure 4: **Ablation.** We show how Flash3D degrades when components are removed. Removing the depth network (4<sup>th</sup> column) results in incorrect geometry (orange wall, corner of the bed). Using only one layer of Gaussians (5<sup>th</sup>) results in holes in renderings due to disocclusions (orange wall, area behind cabinet), although they are not as bad as when simply using depth unprojection (rightmost).

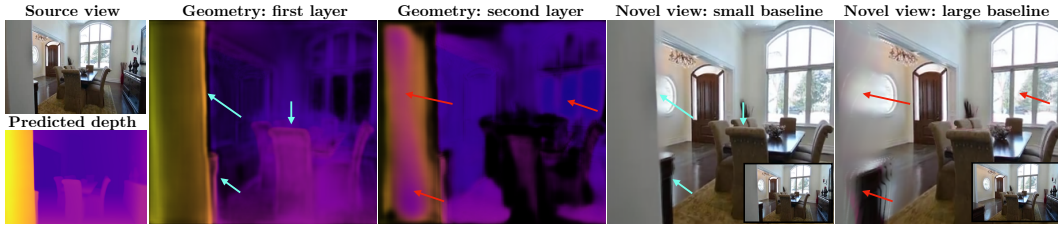


Figure 5: **Analysis of layered Gaussians.** The first layer of Gaussians (second column) represents visible parts where the depth prediction can be used (blue arrows). The second layer (third column) represents the remaining parts of the scene (red arrows): occluded regions (wall, cabinet) and regions where depth prediction is unreliable (windows). Combining the two leads to sharp geometries at small baselines (fourth column) and reasonable reconstructions at large baselines (right column).

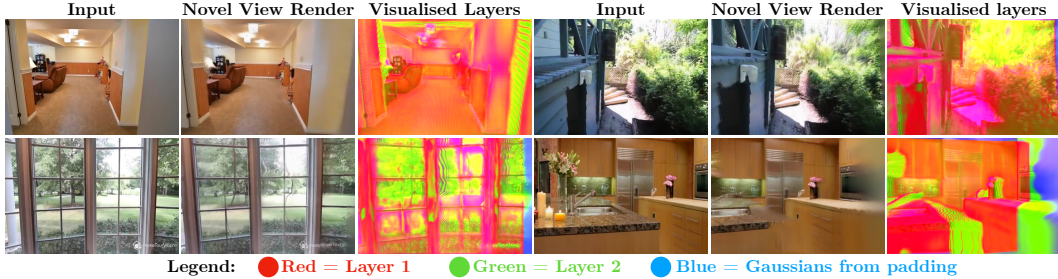


Figure 6: **Analysis of Gaussian allocation.** Gaussians from the first layer (red) are allocated in visible parts, from the second layer (green) in occluded regions (top row, bottom right) and on windows (bottom left) and Gaussians from the padding region (blue) are revealed when camera reveals regions that were not present in the frustum of the input camera.

Table 4: **Ablation Study.** Results for ablating different design choices of our method.

|                              | RE10k – in-domain |              |              | NYU – cross-domain |              |              | KITTI – cross-domain |              |              |
|------------------------------|-------------------|--------------|--------------|--------------------|--------------|--------------|----------------------|--------------|--------------|
|                              | PSNR ↑            | SSIM ↑       | LPIPS ↓      | PSNR ↑             | SSIM ↑       | LPIPS ↓      | PSNR ↑               | SSIM ↑       | LPIPS ↓      |
| Flash3D                      | <b>24.93</b>      | <b>0.833</b> | <b>0.160</b> | <b>25.09</b>       | <b>0.775</b> | <b>0.182</b> | <b>21.96</b>         | <b>0.826</b> | <b>0.132</b> |
| w/o depth net, w/ 2nd layer  | 23.62             | 0.782        | 0.186        | 23.73              | 0.732        | 0.210        | -                    | -            | -            |
| w/o depth net, w/o 2nd layer | 24.01             | 0.806        | 0.176        | 23.98              | 0.750        | 0.207        | -                    | -            | -            |
| w/ depth net, w/o 2nd layer  | 24.45             | 0.825        | 0.163        | 24.83              | 0.767        | 0.190        | 21.50                | 0.812        | 0.141        |
| w/ depth net, unproject only | 22.80             | 0.781        | 0.207        | 22.14              | 0.729        | 0.217        | 20.86                | 0.774        | 0.154        |

## 5 Conclusion

We presented Flash3D, a model that can be trained in just 16h on a single GPU to achieve state-of-the-art results for monocular scene reconstruction. Our formulation allows using a monocular depth estimator as a foundation for full 3D scene reconstruction. As a consequence, the model generalizes very well: it outperforms prior works even when not trained specifically on the target dataset as them. Analyses reveal the interaction mechanisms between the pretrained network and the learned modules, and ablations verify the importance of each component.

## References

- [1] E. Adelson. Layered representations for vision and video. In *ICCV Workshop on the Representation of Visual Scenes*, 1995. [2](#)
- [2] Titas Auciukevicius, Zexiang Xu, Matthew Fisher, Paul Henderson, Hakan Bilen, Niloy J. Mitra, and Paul Guerrero. RenderDiffusion: Image diffusion for 3D reconstruction, inpainting and generation. In *Proc. CVPR*, 2022. [3](#)
- [3] Simon Baker, R. Szeliski, and P. Anandan. A layered approach to stereo reconstruction. In *Proc. CVPR*, 1998. [2](#)
- [4] Stan Birchfield and Carlo Tomasi. Depth discontinuities by pixel-to-pixel stereo. In *Proc. ICCV*, 1998. [1, 3](#)
- [5] Andreas Blattmann, Tim Dockhorn, Sumith Kulal, Daniel Mendelevitch, Maciej Kilian, Dominik Lorenz, Yam Levi, Zion English, Vikram Voleti, Adam Letts, Varun Jampani, and Robin Rombach. Stable video diffusion: Scaling latent video diffusion models to large datasets. *arXiv.cs*, abs/2311.15127, 2023. [2](#)
- [6] B. F. Buxton and H. Buxton. Monocular depth perception from optical flow by space time signal processing. *Phil. Trans. R. Soc. Lond. B*, 218, 1983. [1, 3](#)
- [7] Yuanzhouhan Cao, Zifeng Wu, and Chunhua Shen. Estimating depth from monocular images as classification using deep fully convolutional residual networks. *IEEE Trans. Circuits Syst. Video Techn.*, 28(11):3174–3182, 2018. [1, 3](#)
- [8] Eric R. Chan, Koki Nagano, Matthew A. Chan, Alexander W. Bergman, Jeong Joon Park, Axel Levy, Miika Aittala, Shalini De Mello, Tero Karras, and Gordon Wetzstein. Generative novel view synthesis with 3D-aware diffusion models. In *Proc. ICCV*, 2023. [3, 8](#)
- [9] David Charatan, Sizhe Li, Andrea Tagliasacchi, and Vincent Sitzmann. pixelSplat: 3D Gaussian splats from image pairs for scalable generalizable 3d reconstruction. In *arXiv.cs*, 2023. [2, 3, 6, 7, 8, 16, 17](#)
- [10] Anpei Chen, Zexiang Xu, Fuqiang Zhao, Xiaoshuai Zhang, Fanbo Xiang, Jingyi Yu, and Hao Su. MVSNeRF: Fast generalizable radiance field reconstruction from multi-view stereo. In *Proc. ICCV*, 2021. [3](#)
- [11] Yuedong Chen, Haofei Xu, Chuanxia Zheng, Bohan Zhuang, Marc Pollefeys, Andreas Geiger, Tat-Jen Cham, and Jianfei Cai. MVSplat: efficient 3d gaussian splatting from sparse multi-view images. *arXiv*, 2403.14627, 2024. [2, 3, 6, 8](#)
- [12] Julian Chibane, Aayush Bansal, Verica Lazova, and Gerard Pons-Moll. Stereo radiance fields (SRF): learning view synthesis for sparse views of novel scenes. In *Proc. CVPR*, 2021. [3](#)
- [13] Xiaoliang Dai, Ji Hou, Chih-Yao Ma, Sam S. Tsai, Jialiang Wang, Rui Wang, Peizhao Zhang, Simon Vandenhende, Xiaofang Wang, Abhimanyu Dubey, Matthew Yu, Abhishek Kadian, Filip Radenovic, Dhruv Mahajan, Kunpeng Li, Yue Zhao, Vladan Petrovic, Mitesh Kumar Singh, Simran Motwani, Yi Wen, Yiwen Song, Roshan Sumbaly, Vignesh Ramanathan, Zijian He, Peter Vajda, and Devi Parikh. Emu: Enhancing image generation models using photogenic needles in a haystack. *CoRR*, abs/2309.15807, 2023. [2](#)

- [14] Yilun Du, Cameron Smith, Ayush Tewari, and Vincent Sitzmann. Learning to render novel views from wide-baseline stereo pairs. In *Proc. CVPR*, 2023. 3, 6, 8
- [15] David Eigen, Christian Puhrsch, and Rob Fergus. Depth map prediction from a single image using a multi-scale deep network. In *Proc. NeurIPS*, 2014. 3
- [16] Bill Freeman, Ce Liu, Forrester Cole, Noah Snavely, Richard Tucker, Tali Dekel, and Zhengqi Li. Learning the depths of moving people by watching frozen people. In *Proc. CVPR*, 2019. 1, 3
- [17] Andreas Geiger, Philip Lenz, and Raquel Urtasun. Are we ready for autonomous driving? the KITTI vision benchmark suite. In *Conference on Computer Vision and Pattern Recognition (CVPR)*, 2012. 6
- [18] Andreas Geiger, Philip Lenz, Christoph Stiller, and Raquel Urtasun. Vision meets robotics: The KITTI dataset. *International Journal of Robotics Research (IJRR)*, 2013. 3, 15
- [19] Rohit Girdhar, Mannat Singh, Andrew Brown, Quentin Duval, Samaneh Azadi, Sai Saketh Rambhatla, Akbar Shah, Xi Yin, Devi Parikh, and Ishan Misra. Emu video: Factorizing text-to-video generation by explicit image conditioning. *CoRR*, abs/2311.10709, 2023. 2
- [20] Clément Godard, Oisin Mac Aodha, and Gabriel J. Brostow. Unsupervised monocular depth estimation with left-right consistency. *arXiv.cs*, abs/1609.03677, 2016. 1, 3, 17
- [21] Clément Godard, Oisin Mac Aodha, Michael Firman, and Gabriel J. Brostow. Digging into self-supervised monocular depth prediction. In *Proc. ICCV*, 2019. 3, 17
- [22] Ian J. Goodfellow, Jean Pouget-Abadie, Mehdi Mirza, Bing Xu, David Warde-Farley, Sherjil Ozair, Aaron C. Courville, and Yoshua Bengio. Generative adversarial nets. In *Proc. NeurIPS*, 2014. 8
- [23] Jiatao Gu, Alex Trevithick, Kai-En Lin, Josh M. Susskind, Christian Theobalt, Lingjie Liu, and Ravi Ramamoorthi. NerfDiff: Single-image view synthesis with nerf-guided distillation from 3D-aware diffusion. *arXiv.cs*, abs/2302.10109, 2023. 3
- [24] Kaiming He, Xiangyu Zhang, Shaoqing Ren, and Jian Sun. Deep residual learning for image recognition. In *Proc. CVPR*, 2016. 5, 6, 17
- [25] Philipp Henzler, Jeremy Reizenstein, Patrick Labatut, Roman Shapovalov, Tobias Ritschel, Andrea Vedaldi, and David Novotny. Unsupervised learning of 3d object categories from videos in the wild. In *Proceedings of the IEEE Conference on Computer Vision and Pattern Recognition (CVPR)*, 2021. 3
- [26] Lukas Höllerin, Ang Cao, Andrew Owens, Justin Johnson, and Matthias Nießner. Text2Room: Extracting textured 3D meshes from 2D text-to-image models. In *Proc. ICCV*, 2023. 3
- [27] Yicong Hong, Kai Zhang, Jiuxiang Gu, Sai Bi, Yang Zhou, Difan Liu, Feng Liu, Kalyan Sunkavalli, Trung Bui, and Hao Tan. LRM: Large reconstruction model for single image to 3D. In *Proc. ICLR*, 2024. 3
- [28] Ajay Jain, Matthew Tancik, and Pieter Abbeel. Putting nerf on a diet: Semantically consistent few-shot view synthesis. In *Proc. ICCV*, 2021. 3
- [29] Mohammad Mahdi Johari, Yann Lepoittevin, and François Fleuret. GeoNeRF: generalizing NeRF with geometry priors. In *Proc. CVPR*, 2022. 3
- [30] Abhishek Kar, Christian Häne, and Jitendra Malik. Learning a multi-view stereo machine. In *Proc. NeurIPS*, 2017. 3
- [31] Bernhard Kerbl, Georgios Kopanas, Thomas Leimkühler, and George Drettakis. 3D gaussian splatting for real-time radiance field rendering. *Proc. SIGGRAPH*, 42(4), 2023. 2, 3, 4
- [32] Diederik P. Kingma and Jimmy Ba. Adam: A method for stochastic optimization. *Proc. ICLR*, 2015. 17

- [33] Iro Laina, Christian Rupprecht, Vasileios Belagiannis, Federico Tombari, and Nassir Navab. Deeper depth prediction with fully convolutional residual networks. *arXiv preprint arXiv:1606.00373*, 2016. [1](#), [3](#)
- [34] Katrin Lasinger, René Ranftl, Konrad Schindler, and Vladlen Koltun. Towards robust monocular depth estimation: Mixing datasets for zero-shot cross-dataset transfer. *arXiv*, abs/1907.01341, 2019. [1](#), [3](#)
- [35] Jiahao Li, Hao Tan, Kai Zhang, Zexiang Xu, Fujun Luan, Yinghao Xu, Yicong Hong, Kalyan Sunkavalli, Greg Shakhnarovich, and Sai Bi. Instant3D: Fast text-to-3D with sparse-view generation and large reconstruction model. *Proc. ICLR*, 2024. [2](#)
- [36] Jiaxin Li, Zijian Feng, Qi She, Henghui Ding, Changhu Wang, and Gim Hee Lee. MINE: towards continuous depth MPI with nerf for novel view synthesis. In *Proc. ICCV*, 2021. [1](#), [2](#), [3](#), [6](#), [7](#), [15](#), [16](#), [17](#)
- [37] Ruoshi Liu, Rundi Wu, Basile Van Hoorick, Pavel Tokmakov, Sergey Zakharov, and Carl Vondrick. Zero-1-to-3: Zero-shot one image to 3D object. In *Proc. ICCV*, 2023. [2](#), [3](#)
- [38] Yuan Liu, Sida Peng, Lingjie Liu, Qianqian Wang, Peng Wang, Christian Theobalt, Xiaowei Zhou, and Wenping Wang. Neural rays for occlusion-aware image-based rendering. *arXiv.cs*, abs/2107.13421, 2022. [3](#)
- [39] Nelson L. Max. Optical models for direct volume rendering. *IEEE Trans. Vis. Comput. Graph.*, 1(2):99–108, 1995. doi: 10.1109/2945.468400. [4](#)
- [40] Luke Melas-Kyriazi, Christian Rupprecht, Iro Laina, and Andrea Vedaldi. RealFusion: 360 reconstruction of any object from a single image. In *Proceedings of the IEEE Conference on Computer Vision and Pattern Recognition (CVPR)*, 2023. [2](#), [3](#)
- [41] Luke Melas-Kyriazi, Iro Laina, Christian Rupprecht, Natalia Neverova, Andrea Vedaldi, Oran Gafni, and Filippos Kokkinos. IM-3D: Iterative multiview diffusion and reconstruction for high-quality 3D generation. *arXiv preprint*, abs/2402.08682, 2024. [2](#), [3](#)
- [42] Ben Mildenhall, Pratul P. Srinivasan, Rodrigo Ortiz Cayon, Nima Khademi Kalantari, Ravi Ramamoorthi, Ren Ng, and Abhishek Kar. Local light field fusion: practical view synthesis with prescriptive sampling guidelines. *Proc. SIGGRAPH*, 38(4), 2019. [3](#)
- [43] Ben Mildenhall, Pratul P. Srinivasan, Matthew Tancik, Jonathan T. Barron, Ravi Ramamoorthi, and Ren Ng. NeRF: Representing scenes as neural radiance fields for view synthesis. In *Proc. ECCV*, 2020. [3](#)
- [44] Takeru Miyato, Bernhard Jaeger, Max Welling, and Andreas Geiger. GTA: A geometry-aware attention mechanism for multi-view transformers. *arXiv.cs*, abs/2310.10375, 2023. [3](#)
- [45] Michael Niemeyer, Jonathan T. Barron, Ben Mildenhall, Mehdi S. M. Sajjadi, Andreas Geiger, and Noha Radwan. RegNeRF: Regularizing neural radiance fields for view synthesis from sparse inputs. In *Proc. CVPR*, 2022. [3](#)
- [46] Mertalp Ocal and Armin Mustafa. RealMonoDepth: Self-supervised monocular depth estimation for general scenes. *arXiv.cs*, abs/2004.06267, 2020. [1](#), [3](#)
- [47] Luigi Piccinelli, Yung-Hsu Yang, Christos Sakaridis, Mattia Segu, Siyuan Li, Luc Van Gool, and Fisher Yu. UniDepth: universal monocular metric depth estimation. In *Proc. CVPR*, 2024. [1](#), [2](#), [3](#), [4](#), [6](#)
- [48] Dustin Podell, Zion English, Kyle Lacey, Andreas Blattmann, Tim Dockhorn, Jonas Müller, Joe Penna, and Robin Rombach. SDXL: improving latent diffusion models for high-resolution image synthesis. *arXiv.cs*, abs/2307.01952, 2023. [2](#)
- [49] Ben Poole, Ajay Jain, Jonathan T. Barron, and Ben Mildenhall. DreamFusion: Text-to-3D using 2D diffusion. In *Proc. ICLR*, 2023. [3](#)
- [50] René Ranftl, Alexey Bochkovskiy, and Vladlen Koltun. Vision transformers for dense prediction. *arXiv.cs*, abs/2103.13413, 2021. [3](#)

- [51] Jeremy Reizenstein, Roman Shapovalov, Philipp Henzler, Luca Sbordone, Patrick Labatut, and David Novotny. Common Objects in 3D: Large-scale learning and evaluation of real-life 3D category reconstruction. In *Proc. CVPR*, 2021. 3
- [52] Chris Rockwell, David F. Fouhey, and Justin Johnson. PixelSynth: Generating a 3D-consistent experience from a single image. In *Proc. ICCV*, 2021. 3
- [53] Robin Rombach, Patrick Esser, and Björn Ommer. Geometry-free view synthesis: Transformers and no 3d priors. *arXiv.cs*, abs/2104.07652, 2021. 2
- [54] Olaf Ronneberger, Philipp Fischer, and Thomas Brox. U-net: Convolutional networks for biomedical image segmentation. In *Proc. MICCAI*, 2015. 5, 17
- [55] Mehdi S. M. Sajjadi, Henning Meyer, Etienne Pot, Urs Bergmann, Klaus Greff, Noha Radwan, Suhani Vora, Mario Lucic, Daniel Duckworth, Alexey Dosovitskiy, Jakob Uszkoreit, Thomas A. Funkhouser, and Andrea Tagliasacchi. Scene representation transformer: Geometry-free novel view synthesis through set-latent scene representations. *CoRR*, abs/2111.13152, 2021. 3
- [56] Saurabh Saxena, Abhishek Kar, Mohammad Norouzi, and David J. Fleet. Monocular depth estimation using diffusion models. *arXiv*, 2023. 1, 3
- [57] Johannes Lutz Schönberger and Jan-Michael Frahm. Structure-from-motion revisited. In *Proc. CVPR*, 2016. 15
- [58] J. Shade, S. Gortler, Li wei He, and R. Szeliski. Layered depth images. In *Proc. SIGGRAPH*, 1998. 2
- [59] Shuwei Shao, Zhongcai Pei, Weihai Chen, Xingming Wu, and Zhengguo Li. Nddepth: Normal-distance assisted monocular depth estimation. In *Proc. ICCV*, 2023. 1, 3
- [60] Yichun Shi, Peng Wang, Jianglong Ye, Mai Long, Kejie Li, and Xiao Yang. MVDream: Multi-view diffusion for 3D generation. In *Proc. ICLR*, 2024. 2
- [61] Nathan Silberman, Derek Hoiem, Pushmeet Kohli, and Rob Fergus. Indoor segmentation and support inference from RGBD images. In *Proc. ECCV*, 2012. 3, 6, 15
- [62] Vincent Sitzmann, Michael Zollhöfer, and Gordon Wetzstein. Scene representation networks: Continuous 3D-structure-aware neural scene representations. *Proc. NeurIPS*, 2019. 3
- [63] Vincent Sitzmann, Semon Rezhikov, Bill Freeman, Josh Tenenbaum, and Frédéric Durand. Light field networks: Neural scene representations with single-evaluation rendering. In *Proc. NeurIPS*, 2021. 3
- [64] Pratul P. Srinivasan, Richard Tucker, Jonathan T. Barron, Ravi Ramamoorthi, Ren Ng, and Noah Snavely. Pushing the boundaries of view extrapolation with multiplane images. In *Proc. CVPR*, 2019. 3
- [65] Mohammed Suhail, Carlos Esteves, Leonid Sigal, and Ameesh Makadia. Light field neural rendering. *arXiv.cs*, abs/2112.09687, 2021. 3
- [66] Mohammed Suhail, Carlos Esteves, Leonid Sigal, and Ameesh Makadia. Generalizable Patch-Based neural rendering. In *Proc. ECCV*, 2022. 3
- [67] Stanislaw Szymanowicz, Christian Rupprecht, and Andrea Vedaldi. Viewset diffusion: (0-)image-conditioned 3D generative models from 2D data. In *Proceedings of the International Conference on Computer Vision (ICCV)*, 2023. 3, 8
- [68] Stanislaw Szymanowicz, Christian Rupprecht, and Andrea Vedaldi. Splatter Image: Ultra-fast single-view 3D reconstruction. In *Proceedings of the IEEE Conference on Computer Vision and Pattern Recognition (CVPR)*, 2024. 2, 3, 4, 5, 6, 7, 16
- [69] Jiaxiang Tang, Zhaoxi Chen, Xiaokang Chen, Tengfei Wang, Gang Zeng, and Ziwei Liu. LGM: Large multi-view Gaussian model for high-resolution 3D content creation. *arXiv*, 2402.05054, 2024. 3

- [70] Junshu Tang, Tengfei Wang, Bo Zhang, Ting Zhang, Ran Yi, Lizhuang Ma, and Dong Chen. Make-It-3D: High-fidelity 3d creation from A single image with diffusion prior. *arXiv.cs*, abs/2303.14184, 2023. 3
- [71] Ayush Tewari, Tianwei Yin, George Cazenavette, Semon Rezhikov, Joshua B. Tenenbaum, Frédo Durand, William T. Freeman, and Vincent Sitzmann. Diffusion with forward models: Solving stochastic inverse problems without direct supervision. *arXiv.cs*, abs/2306.11719, 2023. 8
- [72] Zhou Tinghui, Tucker Richard, Flynn John, Fyffe Graham, and Snavely Noah. Stereo magnification: Learning view synthesis using multiplane images. *arxiv*, 2018. 2, 3, 5, 6
- [73] Hung-Yu Tseng, Qinbo Li, Changil Kim, Suhib Alsisan, Jia-Bin Huang, and Johannes Kopf. Consistent view synthesis with pose-guided diffusion models. In *Proc. CVPR*, 2023. 3
- [74] Richard Tucker and Noah Snavely. Single-view view synthesis with multiplane images. In *Proc. CVPR*, 2020. 1, 2, 3, 6, 7, 17
- [75] Shubham Tulsiani, Tinghui Zhou, Alexei A. Efros, and Jitendra Malik. Multi-view supervision for single-view reconstruction via differentiable ray consistency. In *Proc. CVPR*, pages 209–217, 2017.
- [76] Shubham Tulsiani, Richard Tucker, and Noah Snavely. Layer-structured 3d scene inference via view synthesis. In *Proc. ECCV*, 2018. 2, 3, 6, 15
- [77] Dor Verbin, Peter Hedman, Ben Mildenhall, Todd E. Zickler, Jonathan T. Barron, and Pratul P. Srinivasan. Ref-nerf: Structured view-dependent appearance for neural radiance fields. In *Proc. CVPR*, 2022. 3
- [78] Jianyuan Wang, Christian Rupprecht, and David Novotny. PoseDiffusion: solving pose estimation via diffusion-aided bundle adjustment. In *Proc. ICCV*, 2023. 2
- [79] Qianqian Wang, Zhicheng Wang, Kyle Genova, Pratul P. Srinivasan, Howard Zhou, Jonathan T. Barron, Ricardo Martin-Brualla, Noah Snavely, and Thomas A. Funkhouser. Ibrnet: Learning multi-view image-based rendering. In *Proc. CVPR*, 2021. 3
- [80] Shuzhe Wang, Vincent Leroy, Yohann Cabon, Boris Chidlovskii, and Jerome Revaud. DUSt3R: Geometric 3D vision made easy. *arXiv*, 2023. 2
- [81] Zhou Wang, Alan C. Bovik, Hamid R. Sheikh, and Eero P. Simoncelli. Image quality assessment: from error visibility to structural similarity. *IEEE Trans. on Image Processing*, 13(4), 2004. 17
- [82] Daniel Watson, William Chan, Ricardo Martin-Brualla, Jonathan Ho, Andrea Tagliasacchi, and Mohammad Norouzi. Novel view synthesis with diffusion models. In *Proc. ICLR*, 2023. 3
- [83] Christopher Wewer, Kevin Raj, Eddy Ilg, Bernt Schiele, and Jan Eric Lenssen. latentsplat: Autoencoding variational gaussians for fast generalizable 3d reconstruction. *arXiv*, abs/2403.16292, 2024. 2, 3, 6, 7, 8
- [84] Olivia Wiles, Georgia Gkioxari, Richard Szeliski, and Justin Johnson. Synsin: End-to-end view synthesis from a single image. In *Proc. CVPR*, 2020. 3, 6, 7
- [85] Felix Wimbauer, Nan Yang, Christian Rupprecht, and Daniel Cremers. Behind the scenes: Density fields for single view reconstruction. In *Proceedings of the IEEE Conference on Computer Vision and Pattern Recognition (CVPR)*, 2023. 1, 3, 6, 7, 15
- [86] Jamie Wynn and Damiyar Turmukhambetov. DiffusioNeRF: regularizing neural radiance fields with denoising diffusion models. In *Proc. CVPR*, 2023. 3
- [87] Dejia Xu, Yifan Jiang, Peihao Wang, Zhiwen Fan, Humphrey Shi, and Zhangyang Wang. SinNeRF: Training neural radiance fields on complex scenes from a single image. In *Proc. ECCV*, 2022. 3

- [88] Haofei Xu, Anpei Chen, Yuedong Chen, Christos Sakaridis, Yulun Zhang, Marc Pollefeys, Andreas Geiger, and Fisher Yu. MuRF: Multi-baseline radiance fields. *arXiv*, 2312.04565, 2023. 3
- [89] Yinghao Xu, Zifan Shi, Wang Yifan, Hansheng Chen, Ceyuan Yang, Sida Peng, Yujun Shen, and Gordon Wetzstein. GRM: Large gaussian reconstruction model for efficient 3D reconstruction and generation. *arXiv*, 2403.14621, 2024. 3
- [90] Lihe Yang, Bingyi Kang, Zilong Huang, Xiaogang Xu, Jiashi Feng, and Hengshuang Zhao. Depth anything: Unleashing the power of large-scale unlabeled data. In *Proc. CVPR*, 2024. 1, 3
- [91] Wei Yin, Chi Zhang, Hao Chen, Zhipeng Cai, Gang Yu, Kaixuan Wang, Xiaozhi Chen, and Chunhua Shen. Metric3d: Towards zero-shot metric 3d prediction from a single image. In *Proc. ICCV*, 2023. 1
- [92] Alex Yu, Vickie Ye, Matthew Tancik, and Angjoo Kanazawa. PixelNeRF: Neural radiance fields from one or few images. In *Proc. CVPR*, 2021. 2, 3
- [93] Chen Yuedong, Xu Haofei, Wu Qianyi, Zheng Chuanxia, Cham Tat-Jen, and Cai Jianfei. Explicit correspondence matching for generalizable neural radiance fields. *arXiv*, 2304.12294, 2023. 3
- [94] Jason Y. Zhang, Amy Lin, Moneish Kumar, Tzu-Hsuan Yang, Deva Ramanan, and Shubham Tulsiani. Cameras as rays: Pose estimation via ray diffusion. In *Proc. ICLR*, 2024. 2
- [95] Kai Zhang, Sai Bi, Hao Tan, Yuanbo Xiangli, Nanxuan Zhao, Kalyan Sunkavalli, and Zexiang Xu. GS-LRM: large reconstruction model for 3D Gaussian splatting. *arXiv*, 2404.19702, 2024. 2, 3
- [96] Richard Zhang, Phillip Isola, Alexei A. Efros, Eli Shechtman, and Oliver Wang. The unreasonable effectiveness of deep features as a perceptual metric. In *Proc. CVPR*, pages 586–595, 2018. 8
- [97] Chuanxia Zheng and Andrea Vedaldi. Free3D: Consistent novel view synthesis without 3D representation. In *Proceedings of the IEEE Conference on Computer Vision and Pattern Recognition (CVPR)*, 2024. 2, 3
- [98] Tinghui Zhou, Matthew Brown, Noah Snavely, and David G. Lowe. Unsupervised learning of depth and ego-motion from video. In *Proc. CVPR*, 2017. 3

## A Dataset details

**RealEstate10k.** We download the videos from provided links, resulting in above 65,000 videos, as well as the provided camera pose trajectories. Using the provided cameras, we run sparse point cloud reconstruction with COLMAP [57]. We use the test split provided by MINE, and following prior work we evaluate PSNR on novel frames which are 5 and 10 frames ahead of the source frame. In addition, we evaluate on a random frame sampled from an interval of  $\pm 30$  frames. We use the same frames as [36] did for their evaluation. As a result, we evaluate on 3205 frames. We reproduced the results from [36] using their released checkpoint with the common protocol of cropping 5% of the image around the border, achieving scores similar to those presented in the original paper. We confirmed with authors of BTS [85] that this is the commonly used protocol. We do our training and testing at  $256 \times 384$  resolution.

**NYUv2.** We form a benchmark that is similar in nature to RealEstate10k in that it shows indoor scenes, but is visually radically different. We download 80 raw sequences of NYUv2 [61] and run COLMAP [57] on them to recover camera pose trajectories. On each video we sample 3 random source frames and use a random frame uniformly sampled within  $\pm 30$  frames from the source frame, mirroring the protocol of RealEstate10k. We undistort images, and rescale to  $256 \times 384$  resolution.

**KITTI** We evaluate on the Tulsiani test split [76] of the KITTI [18] dataset. The cameras in the KITTI dataset are in metric scale, our network works directly with the provided cameras and scenes without additional preprocessing. For evaluation, following prior work [36, 85] we crop the outer 5% of the images.

## B Baselines and competing methods

### B.1 Depth unprojection

A crucial baseline in our experiments is measuring performance of monocular depth prediction for monocular Novel View Synthesis. In this baseline, we place isotropic 3D Gaussians with fixed opacity without view-dependent effects (i.e. a point cloud with soft point boundaries) at the depths predicted by the monocular depth predictor. We set the Gaussian colours to be a scaled copy from the input view so that  $c_G = \alpha c_{RGB}$  and we initialise  $\alpha = 1.0$ . We initialise Gaussian opacity to be  $\sigma = \text{sigmoid}(\sigma_0)$ , with  $\sigma_0 = 4.0$ , i.e., almost opaque. We test two variants of setting the scale of Gaussians: (1) one where Gaussians have a fixed scale  $s = \exp s_0$  with  $s_0 = -4.5$ , and (2) one where the radius is proportional to depth from camera, allowing the Gaussians to fit inside the ray cast from the pixel:  $s = \exp s_0 d/d_0$ , where  $d$  is metric depth output from UniDepth,  $d_0 = 10.0$  and  $s_0 = -4.5$ . Next, while we determined  $\alpha = 1.0$ ,  $s_0 = -4.5$  and  $\sigma_0 = 4.0$  to be reasonable initialisations, they might not correspond to the highest quality of Novel View Synthesis. Thus, we run gradient-based optimisation of the parameters of this baseline, optimising  $\alpha, s_0, \sigma_0$  to minimise the photometric loss in the source view and 3 novel views (identical to our final model) on the training set. We train these models for X iterations and choose the one with the best performance on validation split. Finally, we evaluate the model with the best  $\alpha, s_0, \sigma_0$  on the test split and report the metrics.

Table 5: **Depth Unprojection Baseline.** We fit hyperparameters of the depth unprojection model via gradient-based optimisation. We try two variants: one with fixed-size Gaussians and one where the Gaussian scale is increased proportionally to depth. Top two rows are before correcting depth-wise unprojection to be from pixel centers instead of pixel corners. All measured with croppint.

| Model           | Backbone   | 5 frames        |                 |                    | 10 frames       |                 |                    | random frame    |                 |                    |
|-----------------|------------|-----------------|-----------------|--------------------|-----------------|-----------------|--------------------|-----------------|-----------------|--------------------|
|                 |            | PSNR $\uparrow$ | SSIM $\uparrow$ | LPIPS $\downarrow$ | PSNR $\uparrow$ | SSIM $\uparrow$ | LPIPS $\downarrow$ | PSNR $\uparrow$ | SSIM $\uparrow$ | LPIPS $\downarrow$ |
| Fixed size      | ConvNeXT-L | 26.47           | 0.864           | 0.120              | 24.08           | 0.808           | 0.173              | 22.60           | 0.774           | 0.211              |
| Fixed size      | ViT-L      | 26.62           | <b>0.867</b>    | <b>0.120</b>       | 24.25           | <b>0.814</b>    | <b>0.172</b>       | 22.78           | <b>0.781</b>    | 0.209              |
| Depth-dependent | ConvNeXT-L | 26.49           | 0.861           | 0.124              | 24.10           | 0.806           | 0.175              | 22.61           | 0.774           | 0.209              |
| Depth-dependent | ViT-L      | <b>26.65</b>    | 0.864           | 0.123              | <b>24.29</b>    | 0.812           | 0.173              | <b>22.80</b>    | <b>0.781</b>    | <b>0.207</b>       |

### B.2 Splatter Image

We implemented the Splatter Image baseline using the same U-Net convolutional neural network with a ResNet-50 backbone as our own method for a fair comparison. We trained it on two NVIDIA A6000 GPUs for a total of 350,000 steps, an order of magnitude more than our proposed Flash3D. Training took 6GPU days, same as reported in [68].

### B.3 MINE

MINE [36] only provided model weights but no inference and evaluation code on RealEstate10K dataset, hence we re-run the inference and evaluation for reproducibility. The results match those reported in [36]. We use the  $N = 64$  model since that is the best one made available by the authors. For evaluation on NYU we use the model trained on Re10k, identically to our method.

### B.4 Two-view methods

When comparing to two-view methods, we ought to choose one of them as our source view. For any method, the most indicative factor of performance on a target frame is the baseline to the source frame. We run this comparison on  $256 \times 256$  without border-cropping for being fully comparable.

### B.5 Probability distribution of Gaussian

An alternative approach to the multiple Gaussians is to predict depth probabilities as in pixelSplat [9]. However, without the estimated depth from the pre-trained depth predictor, the coverage speed is very slow, and the performance is worse in our monocular setting. For a fair comparison, we ablate only on other Gaussian layers, *i.e.*  $K > 1$  of Gaussians. The results are reported in Table 6. The continuous depth offset outperforms the depth probabilities design in pixelSplat.

Table 6: **Ablation Study for Depth Decoder Architectures.** Here, we ablate the probabilistic depth as in pixelSplat [9], but only for the  $K > 1$  of Gaussians.  $-K$  means  $K$  Gaussians per-pixel. Here, cross-domain (CD) denotes that the method was not trained on the dataset being evaluated.

| Method               | CD | KITTI           |                 |                    | NYU |                 |                 |                    |
|----------------------|----|-----------------|-----------------|--------------------|-----|-----------------|-----------------|--------------------|
|                      |    | PSNR $\uparrow$ | SSIM $\uparrow$ | LPIPS $\downarrow$ | CD  | PSNR $\uparrow$ | SSIM $\uparrow$ | LPIPS $\downarrow$ |
| Flash3D (Discrete)-2 | ✓  | 21.35           | 0.805           | 0.153              | ✓   | 24.52           | 0.763           | 0.200              |
| Flash3D (Discrete)-3 | ✓  | 21.50           | 0.814           | 0.136              | ✓   | 24.84           | 0.772           | 0.189              |
| Flash3D (Ours)-2     | ✓  | <b>21.96</b>    | <b>0.826</b>    | <b>0.132</b>       | ✓   | <b>25.09</b>    | <b>0.775</b>    | <b>0.182</b>       |

## C Implementation details

### C.1 Architecture

We base our convolutional network on a ResNet-50 [24] backbone and implement a U-Net [54] encoder-decoder as in [21]. Specifically, a single ResNet encoder is shared by a multiple decoders, one for each layer of appearance parameters as well as depth offset decoders, barring the offset decoder for the first layer as we obtain depth values directly from a pre-trained model.

### C.2 Optimisation

We define the photometric loss following [20] as a weighted sum of  $L_1$  and SSIM [81] terms:

$$\mathcal{L} = \|\hat{J} - J\| + \alpha \text{SSIM}(\hat{J}, J) \quad (2)$$

Differently to prior works [36, 74], we do not use sparse depth supervision.

where  $J$  is a target image,  $\hat{J}$  is a rendering and  $\alpha = 0.85$ . We optimise the network with Adam [32] with batch size 16 and a learning rate of 0.0001 for a total of 40,000 training steps.

### C.3 Scale alignment

Camera poses are typically estimated with COLMAP. These camera poses are in arbitrary scale in each scene. Following prior work, we align the scale of the COLMAP cameras to those estimated by our network using the scale factor computation from [74]. However, if there are outliers in depth estimation (both in our method and baselines), they will impact the scale estimation. As a result, there might be mismatch between the scene reconstruction scale and the scale of camera poses from which novel views are rendered. In consequence, the rendered novel views can be shifted compared to ground truth, which does not significantly impact LPIPS but it does affect PSNR. Thus, at test-time we run scale alignment with RANSAC. We do the same for MINE when evaluating it on the transfer dataset, NYU, since the accuracy of its depth prediction deteriorates in this unseen dataset. When estimating scale we thus use the RANSAC scheme with sample size of 5, 1,000 iterations and threshold 0.1.

## D Limitations

A primary limitation of the proposed approach is due to it being a deterministic, regressive model. This incentivises it to generate blurry renderings in presence of ambiguity, such as when baselines are very large, in occluded regions or when camera moves backward.

Another limitation is that not all occluded surfaces are captured by the reconstructor: the reconstructed 3D models still have some holes. While many of these regions are filled in, some are missed, even when multiple Gaussians are predicted.

Finally, failures in the pre-trained depth estimator are likely to lead to failures in our scene reconstructions, especially if the estimated depth is over-estimated. This is due to the non-negativity of our depth offsets, which therefore cannot recover scene structure closer to the camera than the surface estimated by the pre-trained depth estimator. This makes the model dependent on the quality of a third-party model within the domain of use at inference time.

## E Broader impacts

This work, on monocular scene reconstruction, has potential positive and negative social impacts. On the positive side, the approach significantly reduces the compute and time resources needed to acquire 3D assets in-the-wild, opening the door to consumer applications with positive impacts. For example, the ability to quickly reconstruct one's house to facilitate its sale; the ability to digitally preserve artefacts and sites of cultural heritage; and uses in safe autonomous driving.

On the negative side, this technology has the potential to be used for malicious purposes, such as illegal or unethical tracking and surveillance, or be invasive of someone's privacy, for example by reconstructing their body without their consent. In addition, incorrect predictions may cause harm if used in applications like autonomous driving and robotics, where mis-estimated 3D structures could lead to crashes or suboptimal performance.